

Planning Stable Paths for Concentric Tube Robots

Christos Bergeles, *Member, IEEE*, and Pierre E. Dupont, *Fellow, IEEE*

Abstract—Concentric tube robots are continuum robots that can navigate natural pathways to reach locations deep inside the human body. Their operation is based on rotating and telescopically actuating concentric tubes to achieve robot tip pose control. During tube manipulation, the elastic energy stored in the robot structure may give rise to unstable robot configurations and loss of control. This can occur, in particular, for highly curved and elongated tubes that are required for certain surgical interventions. This paper presents a path planning methodology that allows the utilization of such generally unstable concentric tube robots by ensuring that they operate in their stable configuration regions.

I. INTRODUCTION

Many sites within the human body are inaccessible by traditional straight-shafted minimally invasive robots, as reaching them involves navigation along tortuous paths and also necessitates tool manipulation inside small body cavities. To navigate complex anatomies, continuum robots are a more suitable class of surgical robot [1]–[4].

One type of continuum robots is the concentric tube robot, an example of which under design for choroid plexus cauterisation in the ventricles is shown in Fig. 1. Concentric tube robots have cross sections comparable to needles and catheters, and their operation is based on telescoping and rotating pre-curved tubes to control overall shape as well as tip location. The lumen of the tubes can house additional tubes and wires for controlling articulated tip-mounted tools.

Substantial research has been performed on modeling and control of concentric tube robots [5]–[9], and designs have been proposed for neurosurgery [10], lung procedures [11], and intracardiac beating heart surgery [8], [9], with a recent *in vivo* patent foramen ovale closure in swine [9].

More recent contributions involve the development of algorithms for surgery- and patient-specific robots. In work presented in [12], [13], robot design guidelines from [5] were incorporated in computationally efficient optimization frameworks that estimate the lengths and curvatures of the tubes required to perform beating-heart intracardiac surgery and intra-ventricular neurosurgery. Subsequently, [11] introduced a random-tree-based design algorithm, utilizing a more accurate but computationally expensive kinematic model.

During robot design, path planning has been performed either implicitly or explicitly. Implicit path planning relies on specifying a sufficiently dense set of target configurations that continuity can be used to infer satisfaction of anatomical

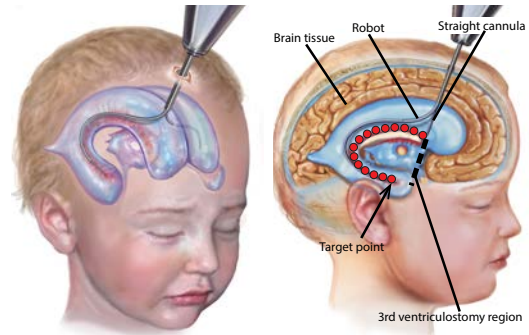


Fig. 1. Robotic cauterization of the choroid plexus in hydrocephalic ventricles to mitigate production of cerebrospinal fluid. Red \circ indicate cauterization points.

constraints when passing between target configurations [12]. Furthermore, the use of designs in which the shape of each robot section is minimally impacted by the configuration of distal sections facilitates implicit path planning during telescopic extension [12]. Explicit path planning during robot design has been considered in [11].

Approaches to explicit path planning include the use of optimization functions to minimize tip pose error with respect to a desired target location while avoiding obstacle collisions [14], [15]. More recently, random-tree algorithms termed Rapidly-Exploring-Roadmaps, characterized by convergence to optimal plans as computational time increases, were introduced [11], [16].

While the methods implemented to date incorporate a complete mechanics model in that they include both bending and twisting of tubes, they do not consider elastic instabilities that arise for certain values of the kinematic input variables (tube rotations and translations). Since these kinematic input values are associated with multiple configurations of the tubes, sudden transitions to lower energy states can occur that involve rapid and uncontrollable untwisting of the tubes. Although it is possible to design tube sets that are globally stable, *i.e.*, the forward kinematic map possesses a unique solution for all input values, this unnecessarily limits the curvature and arc length of robot designs.

The contribution of this paper is to demonstrate that robot designs that exhibit local but not global stability can be useful in addressing clinical procedures. Furthermore, a path planning algorithm is presented that navigates the robot to goal configurations through sequences of local stable configurations that respect anatomical constraints.

The paper is arranged as follows. After introducing the kinematic variables and torsionally compliant mechanics of concentric tube robots in Sec. II, the concept of configuration

This work was supported by the National Institutes of Health under grants R01HL073647 and R01HL087797. C. Bergeles and P. E. Dupont are with the Department of Cardiovascular Engineering, Boston Children's Hospital, Harvard Medical School, 02115 Boston, Massachusetts {firstname.lastname@childrens.harvard.edu}.

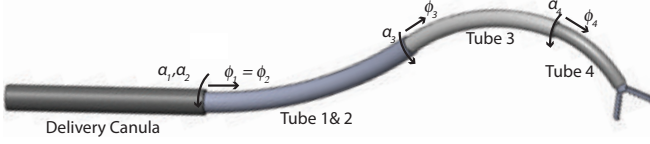


Fig. 2. Concentric tube robot comprising three telescoping sections that can be rotated and translated with respect to each other. The first section, which includes two tubes, is a variable curvature section.

stability and criteria for its satisfaction is examined. Sec. III describes the components of the path planner and its implementation details. The recently introduced RRT* general path planning algorithm is used [17]. Subsequently, Sec. IV investigates the possibility of safely using unstable concentric tube robots and showcases a path planning example. Sec. IV-B presents a specific clinical example from neurosurgery that demonstrates the importance of planning locally stable paths. Conclusions and discussion appear in Sec. V.

II. ROBOT TUBE SET DESIGN AND MODELING

In contrast to standard robots possessing rigid links and discrete joints, concentric tube robots are continuum robots. When their constituent pre-curved tubes are inserted inside each other, their common axis conforms to a mutual resultant curvature. By controlling relative translations and rotations of the tubes at their proximal ends, the shape and length of the robot can be varied (see Fig. 2). Thus, the tubes act as both links and flexure joints.

While it is possible to attempt to design a tube set without any design framework, the problem is high dimensional and the lack of a methodology can make it difficult to verify the optimality of a design. An alternative approach first suggested in [5] that was successfully used for beating-heart intracardiac surgery [8], [9] utilizes the following two design principles to reduce the number of design parameters while also approximately decoupling the motion of each robot section from the others:

1) *Telescoping dominant stiffness*: To produce localized shape changes with respect to arc length, the tube lengths are selected to produce telescoping robot architectures. Furthermore, the outer/proximal tubes possess a composite bending stiffness that dominates the stiffness of the inner/distal tubes, leading to approximate kinematic decoupling between each section and its proximal sections.

2) *Fixed and variable curvature sections*: Each telescoping section has either fixed or variable curvature. A fixed curvature section (single tube) relaxes to its pre-curved shape when extended from the preceding section while a variable curvature section (two tubes) takes on a continuous range of curvatures usually between straight and a maximum value.

A. Mechanics-based Kinematic Model

Elastic models that account for tube twisting and bending, but neglect longitudinal strain and cross section shear have been demonstrated to accurately model concentric tube robots kinematics [5], [7], [18].

Following the approach of [5], a concentric tube robot \mathcal{T} is defined as composed of n tubes with Bishop coordinate

frames defined with respect to each tube. Any non-zero pre-curvature is assumed to be with respect to the y -axis and is denoted by $\hat{u}_{iy}(s)$ in which s is arc length measured along the tube centerline. Each tube is described by its bending stiffness k along the x - and y -axes and by its torsional stiffness $\frac{k}{1+\nu}$ along the z -axis, ν being the tube's Poisson's ratio, assuming a linear isotropic constitutive model. The kinematic variables of each tube are its extension ϕ_i with respect to its proximal section, and its twist angle α_i measured with respect to the outermost (first) tube. A variable curvature section is composed of two tubes that have the same extension. Nomenclature can be found in Table I.

Robot shape is computed by first solving a boundary value problem (BVP) for bending and torsional curvature $\kappa = \{\kappa_x, \kappa_y, \kappa_z\}$ as well as relative twist angle, α , as functions of arc length. These values can be integrated to provide robot shape as a function of arc length. For speed of execution, the equations of [5] are discretized by arc length $s = \{s_j\}, j = 1, \dots, m$, where s_m corresponds to the tip of the robot, and integrated here using Euler's method. While this method has proven sufficient in many practical cases, higher-order methods can also be substituted. The discrete equations are given by:

$$\alpha_i^{s_{j-1}} = [\alpha_i^{s_j} (\kappa_{iz}^{s_j} - \kappa_{1z}^{s_j})] ds \quad (1)$$

$$\kappa_{1z}^{s_{j-1}} = -\frac{1}{k_{1z}} \sum_{i \in \mathcal{T}(s_j) \setminus \{1\}} k_{iz}^{s_j} \kappa_{iz}^{s_j} \quad (2)$$

$$\kappa_{iz}^{s_{j-1}} = \left[\frac{k_{ixy}^{s_j}}{k_{iz}^{s_j}} (\kappa_{ix}^{s_j} \hat{u}_{iy}) \right] ds \quad (3)$$

$$\begin{bmatrix} \kappa_{ix}^{s_j} \\ \kappa_{iy}^{s_j} \\ \kappa_{iz}^{s_j} \end{bmatrix} = \frac{R_z^T(\alpha_i) \sum_{i \in \mathcal{T}(s_j)} k_{ix}^{s_j} R_z(\alpha_i) \begin{bmatrix} 0 \\ \hat{u}_{iy}^{s_j} \end{bmatrix}}{\sum_{i \in \mathcal{T}(s_j)} k_i^{s_j}} \quad (4)$$

and are integrated for $i = 1, \dots, n$, in which $\mathcal{T}(s)$ is the subset of tubes overlapping at arc length s , and R_z denotes rotation around the z -axis. Solving (2)-(4) involves using boundary conditions on kinematic variables $\{\alpha_i^0, \phi_i\}$ at the base of the tubes together with boundary conditions based on zero torques applied at the distal ends of the tubes, $\kappa_{iz}^{d_i} = 0$, where $i = 1, \dots, n$ and d_i is the distal end of tube i .

Given any individual tube curvature, κ_i , and twist angle, α_i , its centerline is calculated using matrix exponentials [5].

B. Elastic Stability

As written, the equations above constitute a BVP since the boundary conditions comprise the relative tube rotations at the robot's base and the torques applied at the distal end of each tube. By redefining the tube rotation boundary conditions to be the relative rotations at the distal ends of the tubes, the problem can be recast as an initial value problem (IVP) and the usual results from differential equations theory can be cited to ensure a solution's existence and uniqueness.

Such cannot be said of the BVP formulation, however, and consequently, a specific set of tube rotations applied at the

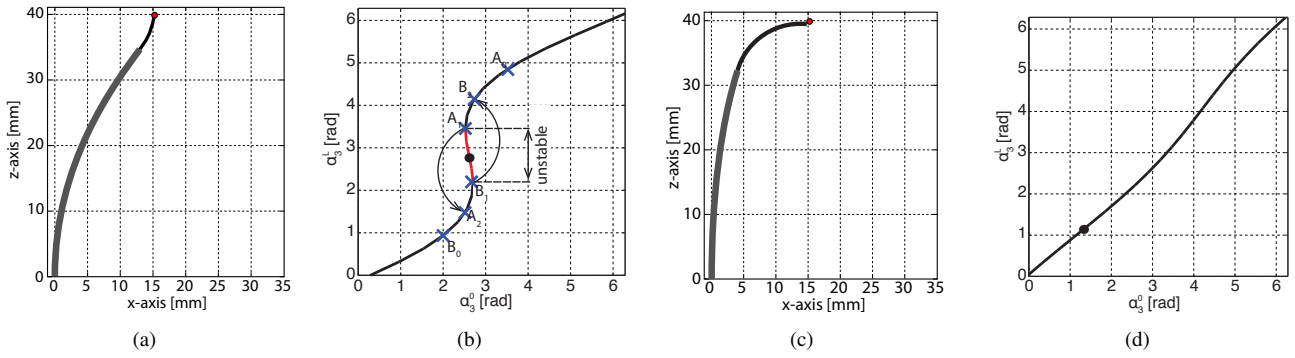


Fig. 3. Example of an unstable [(a), (b)] and a stable configuration [(c), (d)] for a robot comprised of two fixed curvature sections. (a) Unstable robot configuration, (b) Plot of relative base rotation versus relative tip rotation. The black • corresponds to the configuration depicted in (a). (c) Stable robot configuration for same tip position. (d) Relative rotation angle at base versus rotation at tip. The black • indicates the configuration shown in (c).

TABLE I
NOMENCLATURE

Symbol	Description
n	Number of tubes in a robot design
v	Number of variable curvature sections
m	Number of robot centerline discretization points
s	Arc length along centerline of tube or tube set
$\kappa_{ix,y,z}^s$	Curvature components of i th tube due to bending (x, y) and torsion, z , at arc length s
\hat{u}_{iy}	Bending pre-curvature of i th tube about y
ϕ_i	Relative extension of the i th tube or section
d_i	Arc length corresponding to distal end of tube i ,
α_i^s	Relative rotation of the i th tube w.r.t. to the outer tube at s
$k_{ix,y,z}^s$	Stiffness of i th tube in bending (x, y) and torsion, z , at arc length s
ν	Poisson's ratio
R_z	Rotation around the z -axis matrix
D	Stiffness ratio of a section w.r.t. its distal section
\mathcal{T}	Robot tube set
q	Set of kinematic input variables

base may correspond to several sets of relative tube rotations at the distal ends. Each solution may or may not be locally stable under small perturbations to twist angles.

At unstable configurations, small perturbations in relative rotation anywhere along a tube's length can produce large displacements at the distant end. As a specific example, as two curved tubes are rotated away from their aligned configuration, the relative rotation angle at the distal end initially lags the relative rotation angle at the proximal end. If the lag is large enough that tip rotation fails to catch up as the proximal angle passes through π , the tubes will snap through this configuration to one in which the distal rotation leads the proximal value. This has been experimentally and theoretically investigated in [5], [19], but has not been algorithmically formulated for incorporation in path planning.

Solution multiplicity and stability for a pair of tubes can be illustrated graphically by plotting the relative rotation angle at their base, α_i^0 , versus the relative rotation angle of the distal end of the shorter tube, $\alpha_i^{L_i}$. Fig. 3 illustrates a case of solution multiplicity for a two-section robot (Design 1 in Table II). In this design, rotational instability arises when the distal section is sufficiently retracted into the proximal section. Graphically, this results in an s-shaped curve (see Fig. 3(b)). The unstable configurations are marked in red.

Attempting to approach point A_1 from A_0 causes the robot to snap to configuration A_2 . The same behavior is observed for B_0, B_1 and B_2 . This snapping motion is uncontrollable.

Figure 3(c), on the other hand, demonstrates that this robot tip position is stably reachable from a different orientation. This configuration is stable since the distal section is more extended and the curvatures of the robot sections are aligned.

In stable regions the slope of the tangent to the s-curve is positive. Unstable regions: (1) have negative tangent slope, or (2) cannot be reached by passing only through stable configurations, *i.e.*, as the a tube rotates from 0, or 2π , to the operating point α^0 , clockwise, or counter-clockwise, respectively, an unstable configuration is encountered.

Thus, for a given robot configuration, stability is examined through the relationship between each tube's distal and proximal torsional angles as the tube rotates from 0 or 2π to the operating point α^0 :

$$\text{stable} = \begin{cases} \text{if } \alpha^0 \leq \pi \text{ then } \forall 1\alpha^0, 2\alpha^0 \in [0, \alpha^0] : \\ \quad 1\alpha^0 \leq 2\alpha^0 \Rightarrow 1\alpha^d \leq 2\alpha^d \\ \text{or} \\ \text{if } \alpha^0 > \pi \text{ then } \forall 1\alpha^0, 2\alpha^0 \in [\alpha^0, 2\pi] : \\ \quad 1\alpha^0 \leq 2\alpha^0 \Rightarrow 1\alpha^d \leq 2\alpha^d \end{cases} \quad (5)$$

where $1\alpha^0, 2\alpha^0$ are two different relative base angles and $1\alpha^d, 2\alpha^d$ the corresponding distal angles. If every tube pair is stable, then the robot configuration is considered stable. Since unstable motions are dangerous, it is desirable to plan paths that explicitly avoid unstable configurations.

III. PATH PLANNING ALGORITHM

In this paper, RRT* is used to construct optimal paths in robot configuration space. RRT* provides provably asymptotically optimal robot configuration sequences, which makes it appropriate for path planning problems in the medical robotics domain where minimum-distance geometric paths are often preferred. Due to space constraints, readers are invited to seek more information on RRT* in [17].

A. Configuration Space

Each variable curvature section comprises two tubes and is controlled by 3 kinematic variables, namely $q = (\alpha_1^0, \alpha_2^0, \phi)$. Each fixed curvature section is controlled by 2 kinematic variables, namely $q = (\alpha^0, \phi)$. For a robot \mathcal{T} composed of n tubes forming v variable curvature sections:

$$F : \mathbb{R}^{2n+v} \rightarrow \mathbb{R}^{3 \times m} \quad (6)$$

denotes the forward kinematic mapping from configuration space to the Euclidean space occupied by the discretized robot centerline. Path planning involves solving for a stable sequence of configurations that lead from an initial configuration, q_{start} , to a specified goal configuration, q_{goal} , and also satisfy prescribed anatomical constraints.

Path planning in configuration space using randomized sampling algorithms results in computational efficiency since the inverse kinematics, which involve iterative solution of the forward kinematic BVP, need not be calculated.

B. Avoiding Unstable Configurations

Accessing sites deep inside the body can require robot designs with long transmission lengths and multiple highly-curved sections. See, *e.g.*, the examples in [16]. Such designs are highly likely to possess unstable configurations. Since instability occurs only for specific configurations of the tubes, however, it may be possible to employ such designs if it can be shown that the desired tip configurations are reachable via sequences of stable configurations.

For robot tube sets that are designed according to the design rules of Sec. II (sections are fixed or variable curvature and satisfy dominating stiffness condition), the following set of rules can be used to describe stable robot configurations:

- Variable curvature sections are most stable at maximum curvature.
- If a straight dominating proximal section is used, the stability of a variable curvature section increases as it is retracted.
- The stability of adjacent curved sections increases as the distal section is extended.

These rules can be employed to resolve kinematic redundancy during solution of the inverse kinematics and so guide the solution away from unstable configurations. For path planning, however, we wish to avoid computation of the inverse kinematics. Consequently, we operate in configuration space and require potential configurations to satisfy (5).

More specifically, for discrete values of $\alpha_i^{d_i}$ for each tube, i , under examination, equations (2) - (4) are solved to calculate α_i^0 . Subsequently, with the tuples (α^0, α^d) calculated, *i.e.*, with the s-curve known, evaluation of (5) is performed to conclude on the robot stability in a particular configuration.

C. Obstacle Avoidance

After acquiring MRI or CT images for the organs of interest, the anatomical volume is created by image segmentation and is represented as a triangulated surface. Computationally efficient encodings of spatial relationships can be achieved using KD-trees. The vertices of the anatomy are used to

populate a KD-tree, and the tree is queried for the proximity of the concentric tube robot to the anatomy to ensure sufficient separation. All accepted configurations must satisfy the anatomy constraints. Hence, upon convergence of the algorithm, it is guaranteed that all configuration leading from entry configuration to final configuration are both stable and anatomically safe. Since interaction with tissue is prohibited, external forces need not be considered.

D. Implementation Details

The forward kinematic model, used for stability evaluation and interference checking, is implemented as a C++ library. First, stability is evaluated, and, if a configuration is found unstable, it is discarded without interference checking to speed up the computations. Path planning is based on the Open Motion Planning Library [20]. Collision avoidance is based on the KD-tree Nanoflann library [21]. The following examples were computed on an Intel Core 2 Duo, 8GB RAM laptop with Ubuntu 12.04. Calculation time for the path plans is on the order of a few seconds.

IV. EXAMPLES

Path planning examples are presented here for the two robot designs of Table II. To provide an understanding of path planning in terms of robot tip position, the workspaces (reachable tip positions) are depicted for both designs in Fig. 4. These figures were created using uniform sampling of the configuration space, and assume that the robot is extended from a straight rigid cannula aligned with the z axis and with its tip at the origin. The complete workspace is obtained by rotating the depicted xz slice about the z axis.

Since both robot designs are kinematically redundant with respect to tip position, the workspaces can be divided into regions according to the stability of the configuration set corresponding to each tip position. As shown, regions may contain only stable configurations (stable region), may contain both unstable and stable configurations (partially stable) or may consist only of unstable configurations.

Each tip position within the stable regions typically corresponds to a set of stable tip orientations. In partially stable regions, each tip position typically has both stable and unstable orientations associated with it. For example, Figs. 3(a) and 3(c) correspond to the same tip position but different orientations within the partially stable region of Fig. 4(a).

A. Design 1 Planning Example

To clearly illustrate the capability of the proposed approach with respect to path stability, the algorithm was used to plan a path between the labeled points 1 and 2 in Fig. 4(a). In this example, there are no anatomical constraints and these points are representative of the robot moving from a position of initial extension from a straight rigid cannula to a point at the edge of its workspace.

The algorithm was first run without the stability test and then re-run using the stability test of (5). The resulting paths, projected on the workspace plane, are depicted in Fig. 4, where black-dashed line indicates the unstable path, and

TABLE II
EXAMPLE ROBOT DESIGNS

Design 1 (Figs. 3(a), 3(c), 4(a) and 5)		
Section stiffness ratio	$D = 10$	
Section Type	Curvature [1/mm]	Length [mm]
(1) variable curvature	1/40	40
(2) fixed curvature	1/10	20
Design 2 (Figs. 4(b), 1, 6 and 7)		
Section stiffness ratio	$D_{12} = 10, D_{23} = 20$	
Section Type	Curvature [1/mm]	Length [mm]
(1) variable curvature	1/19	58
(2) fixed curvature	1/19	58
(3) fixed curvature	∞	10

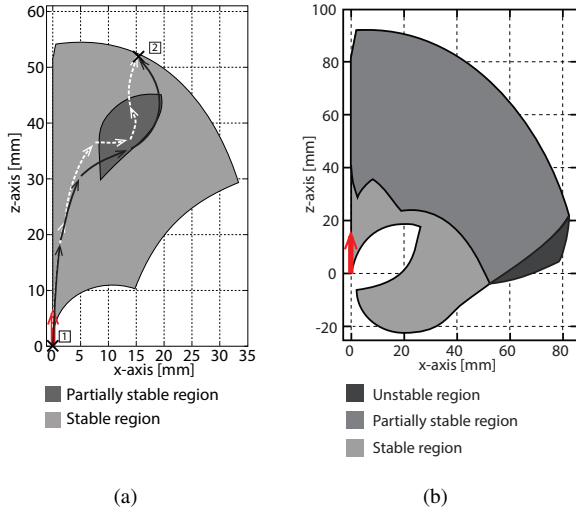


Fig. 4. Robot tip position workspaces for designs of Table II. Complete workspace is obtained by rotating depicted xz slice about the z axis. (a) Design 1 workspace containing stable and partially stable regions. (b) Design 2 workspace containing stable, partially stable and unstable regions. Red arrow indicates robot base.

white dash line the stable path. As shown, without consideration of stability, a planner can select unstable configurations along a path even if the initial and final tip positions lie in completely stable regions. Furthermore, it is not necessary for a stable path to traverse only stable regions; it can also pass through regions of partial stability. The actual path will depend on the anatomical constraints, if present, and will vary due to the random exploration properties of the planning algorithm. Fig. 5 shows the attained robot shapes.

B. Design 2 Planning Example

This robot has been specifically designed for minimally invasive cauterization of the choroid plexus to treat hydrocephalus as shown in Fig. 1. Hydrocephalus is caused by the over-production of cerebrospinal fluid from the choroid plexus of the brain ventricles. Cauterization reduces CSF production, and, in combination with ventriculostomy to enhance fluid drainage, it has been shown to be an effective treatment of hydrocephalus in infants [22].

The robot design was created for the MRI-generated ventricle model of a 10-month old child (Fig. 7) using an algorithm of the type described in [12]. It consists of four

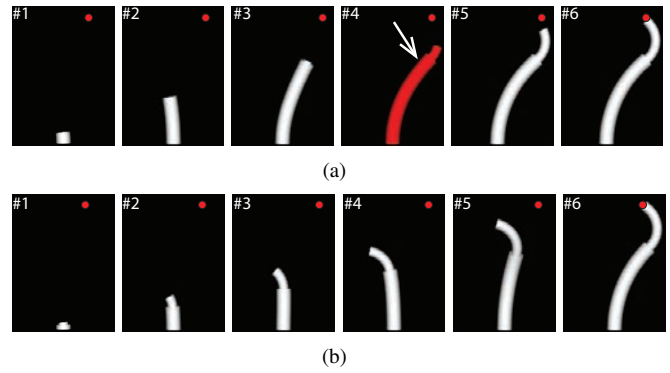


Fig. 5. Paths obtained by planning algorithm for moving from tip position 1 to tip position 2 in Fig. 4(a). (a) Without consideration of path stability. (b) Considering path stability. Unstable robot configurations shown in red.

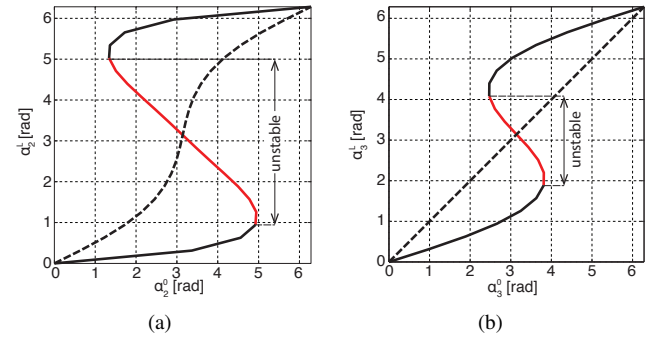


Fig. 6. Design 2 instabilities. (a) Relative base and tip rotations of the variable curvature section, (b) Relative base and tip rotations for the middle fixed-curvature section. Two curves correspond to two extension lengths.

sections from base to tip: a straight rigid cannula, a variable curvature section, a fixed curvature section and a distal fixed-curvature (straight) monopolar cauterization wire. Procedural safety requires stable navigation of the robot from the entry location shown in Fig. 1 to all marked cauterization points.

Due to the length and high curvature of this design, it exhibits two types of instability. The first is associated with straightening of the proximal variable curvature section. The second is associated with rotation of the middle curved section while retracted inside the proximal section.

These instabilities are shown graphically in Fig. 6. The solid curve in Fig. 6(a) corresponds to the variable curvature section being fully extended. It can be seen that at this extension it can only be partially straightened. The dashed curve corresponds to 40% of the variable curvature section extended from a straight rigid base cannula and demonstrates that full straightening is possible. The solid curve in Fig. 6(b) corresponds to an 80% extension of the middle fixed-curvature section and demonstrates that this section cannot be fully rotated. At full extension (dashed curve), however, full rotation is possible.

Fig. 4(b) shows that most of the workspace is only partially stable. Consequently, accounting for stability during path planning is critically important. The proposed algorithm was applied to generating a stable path leading from the insertion site to the most distal cauterization target, indicated with an arrow in Fig. 1. The resulting paths, generated with and

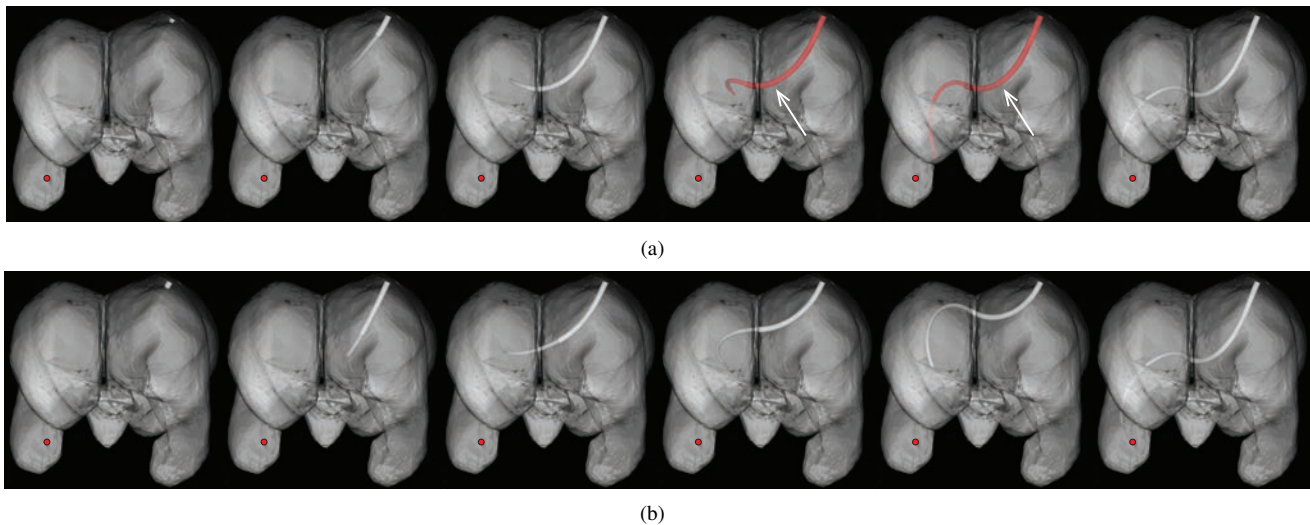


Fig. 7. Paths leading from base cannula insertion point to distal cauterization target. (a) Without consideration of path stability, (b) Considering path stability. Unstable configurations shown in red and indicated by arrows. Red circle marks goal position.

without stability testing, are depicted in Fig. 7. In the top row of Fig. 7, the first section, a variable curvature section, is straightened and extended. This causes an instability to occur. By incorporating the stability criterion, the variable curvature section is kept retracted and curved until the second section is fully extended. The interaction of the variable curvature section with the straight transmission length of second section results in stable configurations.

V. CONCLUSIONS AND DISCUSSION

While the existence of unstable concentric tube robot configurations has been previously noted, the consideration of stability in robot design and path planning has not been previously addressed. This is likely due to most early efforts being devoted to theoretical modeling as opposed to applying concentric tube robots to specific clinical procedures.

The examples considered in this paper reveal that it is not necessary to design tube sets that are globally stable. In fact, procedural and anatomical constraints may preclude the use of such designs. By understanding the sources of instability, however, and incorporating these concepts into workspace modeling, robot design and path planning, locally stable designs can be safely employed in surgery.

REFERENCES

- [1] K. W. Kwok, V. Vitiello, and G.-Z. Yang, "Control of articulate snake robot under dynamic active constraints," *Int. Conf. Medical Image Computing and Computer Assisted Intervention*, pp. 229–236, 2010.
- [2] J. Jayender, M. Azizian, and R. V. Patel, "Autonomous image-guided robot-assisted active catheter insertion," *IEEE Trans. Robotics*, vol. 24, no. 4, pp. 858–871, 2008.
- [3] N. Simaan, K. Xu, W. Wei, A. Kapoor, P. Kazanzides, R. H. Taylor, and P. Flint, "Design and integration of a telerobotic system for minimally invasive surgery of the throat," *Int. J. Robotics Research*, vol. 28, no. 9, pp. 1134–1153, 2009.
- [4] E. Shamma, A. Wolf, and H. Choset, "Three degrees-of-freedom joint for spatial hyper-redundant robots," *Mechanism and Machine Theory*, no. 41, pp. 170–190, 2006.
- [5] P. E. Dupont, *et al.*, "Design and control of concentric-tube robots," *IEEE Trans. Robotics*, vol. 26, no. 2, pp. 209–225, 2010.
- [6] D. C. Rucker, R. J. Webster III, G. Chirikjian, and N. J. Cowan, "Equilibrium conformations of concentric-tube continuum robots," *Int. J. Robotics Research*, vol. 29, no. 10, pp. 1263–1280, 2010.
- [7] J. Lock, G. Laing, M. Mahvash, and P. E. Dupont, "Quasistatic modeling of concentric tube robots with external loads," *IEEE/RSJ Int. Conf. Intelligent Robots and Systems*, pp. 2325–2332, 2010.
- [8] A. Gosline, N. V. Vasilyev, A. Veeramani, M. T. Wu, G. Schmitz, R. Chen, V. Arabagi, P. J. del Nido, and P. E. Dupont, "Metal-MEMS tools for beating-heart tissue removal," *IEEE Int. Conf. Robotics and Automation*, pp. 1921–1936, 2012.
- [9] A. Gosline, N. V. Vasilyev, E. Butler, C. Folk, A. Cohen, R. Chen, N. Lang, P. J. del Nido, and P. E. Dupont, "Percutaneous intracardiac beating-heart surgery using metal MEMS tissue approximation tools," *Int. J. Robotics Research*, vol. 31, no. 9, pp. 1081–1093, 2012.
- [10] J. Burgner, P. J. Swaney, D. C. Rucker, H. B. Gilbert, P. R. Russel III, K. D. Weaver, and R. J. Webster III, "A bimanual teleoperated system for endonasal skull base surgery," *IEEE/RSJ Int. Conf. Intelligent Robots and Systems*, pp. 2517–2523, 2011.
- [11] L. G. Torres, R. J. Webster III, and R. Alterovitz, "Task-oriented design of concentric tube robots using mechanics-based models," *IEEE/RSJ Int. Conf. Intelligent Robots and Systems*, pp. 4449–4455, 2012.
- [12] C. Bedell, J. Lock, A. Gosline, and P. E. Dupont, "Design optimization of concentric tube robots based on task and anatomical constraints," *IEEE Int. Conf. Robotics and Automation*, pp. 398–403, 2011.
- [13] T. Anor, J. R. Madsen, and P. E. Dupont, "Algorithms for design of continuum robots using the concentric tubes approach: a neurosurgical example," *IEEE Int. Conf. Rob. Aut.*, pp. 667–673, 2011.
- [14] L. A. Lyons, R. J. Webster III, and R. Alterovitz, "Motion planning for active cannulas," *IEEE/RSJ Int. Conf. Intel. Rob. Sys.*, 2009.
- [15] L. Lyons, R. J. Webster III, and R. Alterovitz, "Planning active cannula configurations through tubular anatomy," *IEEE Int. Conf. Robotics and Automation*, pp. 2082–2087, 2010.
- [16] L. G. Torres and R. Alterovitz, "Motion planning for concentric tube robots using mechanics-based models," *IEEE/RSJ Int. Conf. Intelligent Robots and Systems*, pp. 5153–5159, 2011.
- [17] S. Karaman and E. Frazzoli, "Sampling-based algorithms for optimal motion planning," *Int. J. Rob. Res.*, vol. 30, no. 7, pp. 846–894, 2011.
- [18] D. C. Rucker, B. A. Jones, and R. J. Webster III, "A geometrically exact model for externally-loaded concentric-tube continuum robots," *IEEE Trans. Robotics*, vol. 26, no. 5, pp. 769–780, 2010.
- [19] R. J. Webster III, *et al.*, "Mechanics of precurved-tube continuum robots," *IEEE Trans. Robotics*, vol. 25, no. 1, pp. 67–78, 2009.
- [20] I. A. Şucan, M. Moll, and L. E. Kavraki, "The Open Motion Planning Library," *IEEE Robotics and Automation Magazine*, vol. 19, no. 4, pp. 72–82, December 2012, <http://ompl.kavrakilab.org>.
- [21] (2013) Nanoflann library. [Online].
- [22] B. Warf, "Endoscopic third ventriculostomy and choroid plexus cauterization for pediatric hydrocephalus," *J. Clinical Neurosurgery*, vol. 54, pp. 78–82, 2007.